Link to published version (if available):

Link to publication record in Explore Bristol Research
PDF-document

University of Bristol - Explore Bristol Research
General rights

Demonstration of diamond microlens structures by a three-dimensional (3D) dual-mask method

YANFENG ZHANG,[1,*] YUNXIAO LI,[1] LIN LIU,[1] CHUNCHUAN YANG,[1] YUJIE CHEN,[1] AND SIYUAN YU[1,2]

[1]*State Key Laboratory of Optoelectronic Materials and Technologies, School of Electronics and Information Technology, Sun Yat-sen University, Guangzhou 510275, China*
[2]*Photonics Group, Merchant Venturers School of Engineering, University of Bristol, Bristol BS8 1UB, UK*
[*]zhangyf33@mail.sysu.edu.cn

Abstract: Diamond is a promising platform for quantum information technologies (QITs) mainly due to the properties of color centers including spin read-out, magnetic field sensing, and entanglement between different nitrogen-vacancy (NV) centers. High photon collection efficiency is essential for a high fidelity optical single-shot readout of electronic spin in the color center. To avoid total internal reflection, sculpting solid immersion lenses in the diamond surface is an ideal natural choice. Three-dimensional (3D) microstructures can be made in a photoresist material by a special lithography method. These structures can be subsequently transferred into silicon, diamond or other semiconductors by plasma etching with appropriate selectivity. However, this method cannot be directly implemented into making large height diamond microlenses where the selectivity between diamond and the photoresist is very low. In this work, we propose and demonstrate a dual mask method to achieve an overall high selectivity between diamond and photoresist via the interlayer of single crystalline silicon. By tuning the process parameters of the two etching steps, diamond micro-lenses with large variable height are successfully demonstrated.

References and links

1. B. J. M. Hausmann, I. Bulu, V. Venkataraman, P. Deotare, and M. Loncar, "Diamond nonlinear photonics," Nat. Photon. **8**, 369–374 (2014).
2. K. Beha, H. Fedder, M. Wolfer, M. C. Becker, P. Siyushev, M. Jamali, A. Batalov, C. Hinz, J. Hees, L. Kirste, H. Obloh, E. Gheeraert, B. Naydenov, I. Jakobi, F. Dolde, S. Pezzagna, D. Twittchen, M. Markham, D. Dregely, H. Giessen, J. Meijer, F. Jelezko, C. E. Nebel, R. Bratschitsch, A. Leitenstorfer, and J. Wrachtrup, "Diamond nanophotonics," Beilstein J. Nanotech. **3**, 895–908 (2012).
3. I. Aharonovich, A. D. Greentree, and S. Prawer, "Diamond photonics," Nat. Photon. **5**, 397–405 (2011).
4. A. D. Greentree, B. A. Fairchild, F. M. Hossain, and S. Prawer, "Diamond integrated quantum photonics," Mater. Today **11**, 22–31 (2008).
5. R. Brouri, A. Beveratos, J. Poizat, and P. Grangier, "Photon antibunching in the fluorescence of individual color centers in diamond," Opt. Lett. **25**, 1294–1296 (2000).
6. F. Jelezko and J. Wrachtrup, "Single defect centres in diamond: A review," Phys. Status Solidi A **203**, 3207–3225 (2006).
7. C. Kurtsiefer, S. Mayer, P. Zarda, and H. Weinfurter, "Stable solid-state source of single photons," Phys. Rev. Lett. **85**, 290–293 (2000).
8. T. Iwasaki, F. Ishibashi, Y. Miyamoto, Y. Doi, S. Kobayashi, T. Miyazaki, K. Tahara, K. D. Jahnke, L. J. Rogers, B. Naydenov, F. Jelezko, S. Yamasaki, S. Nagamachi, T. Inubushi, N. Mizuochi, and M. Hatano, "Germanium-vacancy single color centers in diamond," Sci. Rep. **5**, 12882 (2015).
9. F. Dolde, H. Fedder, M. W. Doherty, T. Noebauer, F. Rempp, G. Balasubramanian, T. Wolf, F. Reinhard, L. C. L. Hollenberg, F. Jelezko, and J. Wrachtrup, "Electric-field sensing using single diamond spins," Nat. Phys. **7**, 459–463 (2011).
10. L. Jiang, J. S. Hodges, J. R. Maze, P. Maurer, J. M. Taylor, D. G. Cory, P. R. Hemmer, R. L. Walsworth, A. Yacoby, A. S. Zibrov, and M. D. Lukin, "Repetitive readout of a single electronic spin via quantum logic with nuclear spin ancillae," Science **326**, 267–272 (2009).
11. G. Waldherr, P. Neumann, S. F. Huelga, F. Jelezko, and J. Wrachtrup, "Violation of a temporal Bell inequality for single spins in a diamond defect center," Phys. Rev. Lett. **107**, 090401 (2011).

12. H. Bernien, B. Hensen, W. Pfaff, G. Koolstra, M. S. Blok, L. Robledo, T. H. Taminiau, M. Markham, D. J. Twitchen, L. Childress, and R. Hanson, "Heralded entanglement between solid-state qubits separated by three metres," Nature **497**, 86–90 (2013).

13. W. Pfaff, B. J. Hensen, H. Bernien, S. B. van Dam, M. S. Blok, T. H. Taminiau, M. J. Tiggelman, R. N. Schouten, M. Markham, D. J. Twitchen, and R. Hanson, "Unconditional quantum teleportation between distant solid-state quantum bits," Science **345**, 532–535 (2014).

14. B. Hensen, H. Bernien, A. E. Dreau, A. Reiserer, N. Kalb, M. S. Blok, J. Ruitenberg, R. F. L. Vermeulen, R. N. Schouten, C. Abellan, W. Amaya, V. Pruneri, M. W. Mitchell, M. Markham, D. J. Twitchen, D. Elkouss, S. Wehner, T. H. Taminiau, and R. Hanson, "Loophole-free Bell inequality violation using electron spins separated by 1.3 kilometres," Nature **526**, 682–686 (2015).

15. W. B. Gao, A. Imamoglu, H. Bernien, and R. Hanson, "Coherent manipulation, measurement and entanglement of individual solid-state spins using optical fields," Nat. Photon. **9**, 363–373 (2015).

16. L. Robledo, L. Childress, H. Bernien, B. Hensen, P. F. A. Alkemade, and R. Hanson, "High-fidelity projective read-out of a solid-state spin quantum register," Nature **477**, 574–578 (2011).

17. J. P. Hadden, J. P. Harrison, A. C. Stanley-Clarke, L. Marseglia, Y. L. D. Ho, B. R. Patton, J. L. O'Brien, and J. G. Rarity, "Strongly enhanced photon collection from diamond defect centers under microfabricated integrated solid immersion lenses," Appl. Phys. Lett. **97**, 241901 (2010).

18. T. M. Babinec, B. J. M. Hausmann, M. Khan, Y. Zhang, J. R. Maze, P. R. Hemmer, and M. Loncar, "A diamond nanowire single-photon source," Nat. Nanotech. **5**, 195–199 (2010).

19. S. A. Momenzadeh, R. J. Stoehr, F. F. de Oliveira, A. Brunner, A. Denisenko, S. Yang, F. Reinhard, and J. Wrachtrup, "Nanoengineered diamond waveguide as a robust bright platform for nanomagnetometry using shallow nitrogen vacancy centers," Nano Lett. **15**, 165–169 (2015).

20. I. Aharonovich, J. C. Lee, A. P. Magyar, D. O. Bracher, and E. L. Hu, "Bottom-up engineering of diamond micro- and nano-structures," Laser Photon. Rev. **7**, L61–L65 (2013).

21. S. Furuyama, K. Tahara, T. Iwasaki, M. Shimizu, J. Yaita, M. Kondo, T. Kodera, and M. Hatano, "Improvement of fluorescence intensity of nitrogen vacancy centers in self-formed diamond microstructures," Appl. Phys. Lett. **107**, 163102 (2015).

22. M. P. Hiscocks, K. Ganesan, B. C. Gibson, S. T. Huntington, F. Ladouceur, and S. Prawer, "Diamond waveguides fabricated by reactive ion etching," Opt. Express **16**, 19512–19519 (2008).

23. Y. Zhang, L. McKnight, Z. Tian, S. Calvez, E. Gu, and M. D. Dawson, "Large cross-section edge-coupled diamond waveguides," Diam. Relat. Mater. **20**, 564–567 (2011).

24. D. Le Sage, L. M. Pham, N. Bar-Gill, C. Belthangady, M. D. Lukin, A. Yacoby, and R. L. Walsworth, "Efficient photon detection from color centers in a diamond optical waveguide," Phys. Rev. B **85**, 121202 (2012).

25. B. Khanaliloo, M. Mitchell, A. C. Hryciw, and P. E. Barclay, "High-Q monolithic diamond microdisks fabricated with quasi-isotropic etching," Nano Lett. **15**, 5131–5136 (2015).

26. B. J. M. Hausmann, B. J. Shields, Q. Quan, Y. Chu, N. P. de Leon, R. Evans, M. J. Burek, A. S. Zibrov, M. Markham, D. J. Twitchen, H. Park, M. D. Lukin, and M. Loncar, "Coupling of NV centers to photonic crystal nanobeams in diamond," Nano Lett. **13**, 5791–5796 (2013).

27. A. Faraon, P. E. Barclay, C. Santori, K.-M. C. Fu, and R. G. Beausoleil, "Resonant enhancement of the zero-phonon emission from a colour centre in a diamond cavity," Nat. Photon. **5**, 301–305 (2011).

28. J. Riedrich-Moeller, L. Kipfstuhl, C. Hepp, E. Neu, C. Pauly, F. Muecklich, A. Baur, M. Wandt, S. Wolff, M. Fischer, S. Gsell, M. Schreck, and C. Becher, "One- and two-dimensional photonic crystal microcavities in single crystal diamond," Nat. Nanotech. **7**, 69–74 (2012).

29. B. J. M. Hausmann, B. Shields, Q. Quan, P. Maletinsky, M. McCutcheon, J. T. Choy, T. M. Babinec, A. Kubanek, A. Yacoby, M. D. Lukin, and M. Loncar, "Integrated diamond networks for quantum nanophotonics," Nano Lett. **12**, 1578–1582 (2012).

30. I. Bayn, B. Meyler, J. Salzman, and R. Kalish, "Triangular nanobeam photonic cavities in single-crystal diamond," New J. Phys. **13**, 025018 (2011).

31. P. E. Barclay, K.-M. Fu, C. Santori, and R. G. Beausoleil, "Hybrid photonic crystal cavity and waveguide for coupling to diamond NV-centers," Opt. Express **17**, 9588–9601 (2009).

32. K. M. C. Fu, C. Santori, P. E. Barclay, I. Aharonovich, S. Prawer, N. Meyer, A. M. Holm, and R. G. Beausoleil, "Coupling of nitrogen-vacancy centers in diamond to a GaP waveguide," Appl. Phys. Lett. **93**, 234107 (2008).

33. N. Thomas, R. J. Barbour, Y. Song, M. L. Lee, and K.-M. C. Fu, "Waveguide-integrated single-crystalline GaP resonators on diamond," Opt. Express **22**, 13555–13564 (2014).

34. M. Shinoda, K. Saito, T. Kondo, A. Nakaoki, M. Furuki, M. Takeda, M. Yamamoto, T. Schaich, B. Van Oerle, H. Godfried, P. Kriele, E. Houwman, W. Nelissen, G. Pels, and P. Spaaij, "High-density near-field readout using diamond solid immersion lens," J. J. Appl. Phys. Part 1 **45**, 1311–1313 (2006).

35. M. Jamali, I. Gerhardt, M. Rezai, K. Frenner, H. Fedder, and J. Wrachtrup, "Microscopic diamond solid-immersion-lenses fabricated around single defect centers by focused ion beam milling," Rev. Sci. Instrum. **85**, 123703 (2014).

36. D. G. Monticone, J. Forneris, M. Levi, A. Battiato, F. Picollo, P. Olivero, P. Traina, E. Moreva, E. Enrico, G. Brida, I. P. Degiovanni, M. Genovese, G. Amato, and L. Boarino, "Single-photon emitters based on NIR color centers in diamond coupled with solid immersion lenses," Internation. J. Quan. Infor. **12**, 1560011 (2014).

37. L. J. Rogers, K. D. Jahnke, T. Teraji, L. Marseglia, C. Mueller, B. Naydenov, H. Schauffert, C. Kranz, J. Isoya, L. P.

McGuinness, and F. Jelezko, "Multiple intrinsically identical single-photon emitters in the solid state," Nat. Commun. **5**, 4739 (2014).

38. L. Marseglia, J. P. Hadden, A. C. Stanley-Clarke, J. P. Harrison, B. Patton, Y.-L. D. Ho, B. Naydenov, F. Jelezko, J. Meijer, P. R. Dolan, J. M. Smith, J. G. Rarity, and J. L. O'Brien, "Nanofabricated solid immersion lenses registered to single emitters in diamond," Appl. Phys. Lett. **98**, 133107 (2011).

39. H. Choi, E. Gu, C. Liu, C. Griffin, J. Girkin, I. Watson, and M. Dawson, "Fabrication of natural diamond microlenses by plasma etching," J. Vac. Sci. Tech. B **23**, 130–132 (2005).

40. T.-F. Zhu, J. Fu, W. Wang, F. Wen, J. Zhang, R. Bu, M. Ma, and H.-X. Wang, "Fabrication of diamond microlenses by chemical reflow method," Opt. Express **25**, 1185–1192 (2017).

41. O. Fox, L. Alianelli, A. Malik, I. Pape, P. May, and K. Sawhney, "Nanofocusing optics for synchrotron radiation made from polycrystalline diamond," Opt. Express **22**, 7657–7668 (2014).

42. E. Woerner, C. Wild, W. Mueller-Sebert, and P. Koidl, "CVD-diamond optical lenses," Diam. Relat. Mater. **10**, 557–560 (2001).

43. Y. Li, Y. Zhang, L. Liu, and C. Yang, "Diamond micro-lenses with variable height using self-assembly silica-microsphere-monolayer as etching mask," Mater. Today Commun. **11**, 119–122 (2017).

44. L. Li, I. Bayn, M. Lu, C.-Y. Nam, T. Schroeder, A. Stein, N. C. Harris, and D. Englund, "Nanofabrication on unconventional substrates using transferred hard masks," Sci. Rep. **5**, 7802 (2015).

45. A. F. Khokhryakov, Y. N. Palyanov, I. N. Kupriyanov, Y. M. Borzdov, and A. G. Sokol, "Effect of nitrogen impurity on the dislocation structure of large HPHT synthetic diamond crystals," J. Cryst. Growth **386**, 162–167 (2014).

46. Y. Zhang, "Diamond and GaN waveguides and microstructures for integrated quantum photonics," Ph.D. thesis, University of Strathclyde (2012).

47. P. Forsberg and M. Karlsson, "High aspect ratio optical gratings in diamond," Diam. Relat. Mater. **34**, 19–24 (2013).

1. Introduction

Diamond photonic structures in diamond are key to most of its application in quantum information technologies (QITs) as well as classical technology [1–4]. The exquisite properties of diamond color centers [5, 6] have led to the realization of solid state single photon source [7, 8], quantum metrology [9, 10], quantum entanglement and teleportation [11–15]. The mutual requirement of utilizing diamond color centers is the high photon collection efficiency, which is essential for high fidelity optical single-shot readout of electronic spin in color center [16]. However, the collection efficiencies are limited by the total internal reflection (TIR) between the high refractive index diamond and its low-index surrounding. Many efforts are put into this area and progresses have been made to overcome the TIR in bulk diamonds. These include solid immersion lenses [17], vertical nanowire and pillars [18, 19], bottom up structures [20, 21], waveguides [22–24], optical cavities [1, 25–30], and hybrid photonic structures [31–33]. Among them, sculpting solid immersion lenses in the diamond surface is an ideal natural choice and have been used in recent experiment of loophole-free Bell inequality violation [14].

Up to now, most of diamond solid immersion lenses are fabricated through focused ion beam milling [17, 34–37] or mechanical polishing [38], which are not scalable for future QITs. Large scale diamond microlens array has been fabricated through photoresist reflow and plasma etching [39, 40]. However, due to the poor selectivity between diamond and photoresist, the diamond lens made through this method are very shallow, typically less than 2 μm height for lens with diameter of tens microns. Therefore, the large scale fabrication of hemisphere diamond microlens array is critical for future quantum and classical applications. Note that nanocrystalline diamond lenses have been realized on substrates deposited with chemical vapor deposition (CVD) diamond thin films [41, 42]. Compared with nanocrystalline diamond, color center in single crystal diamond has better optical properties. Using self-assembly silica-microsphere-monolayer as hard etching mask can fabricate single crystal diamond microlens arrays [43]. However, the sizes of microlenses are limited to silica microsphere diameters (usually only several microns).

In this work, we introduce a 3D dual-mask transfer method to fabricate single crystal diamond microlenses. Firstly, we produced silicon mask with 3D lenses pattern via photoresist reflow technique and fluorine-based plasma etching. Then, the silicon mask was picked up and placed on the diamond substrate surface. Finally, the pattern was transferred into diamond substrate via oxygen-based plasma etching. Relationship between gas mixture ratios and etching selectivity
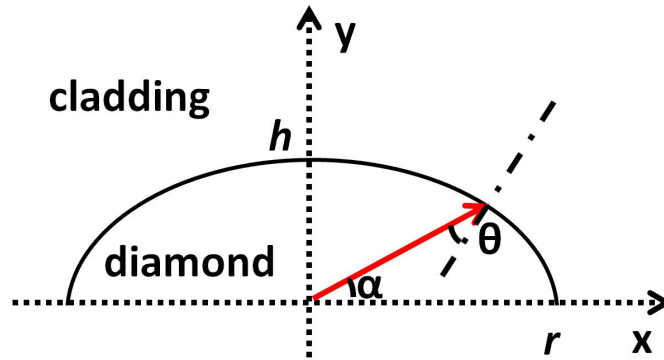
Fig. 1. Diagram of an ideal semi-ellipsoid.

was studied. Scanning electron microscope (SEM) and surface profiler have been used to verify the profiles of the micro-lenses.

2. Design

Suppose the diamond microlens surface profile is an ideal semi-ellipsoid. As shown in Fig.1, its surface curve can be expressed as

$$\frac{x^2}{r^2} + \frac{y^2}{h^2} = 1 \qquad (y > 0) \tag{1}$$

where r is the radius of microlens and h is the height of microlens. Suppose an NV center located at the center of the microlens, i.e. at the coordinate origin. When the emitted photon angle $\alpha = \pm arctan(\frac{h}{r})$, θ reaches its maximum value. Based on ray analysis of light, in order to avoid total internal reflection of photon emitted from NV centers occuring on the entire semi-ellipsoid surface, parameters r and h should satisfy

$$\frac{1 - \frac{h^2}{r^2}}{1 + \frac{h^2}{r^2}} \quad < \quad \frac{n_{\text{cladding}}}{n_{\text{diamond}}} \tag{2}$$

Put $n_{\text{cladding}} = 1$ and $n_{\text{diamond}} = 2.4$ into Eq.(2), we can obtain the following equation

$$h \quad > \quad 0.64 \cdot r \tag{3}$$

As will be demonstrated in the following, we can tune the diamond microlens height to satisfy Eq.(3), which is our design rule for fabricating microlenses.

3. Fabrication process and results

The fabrication process of our method includes photolithography, photoresist reflow, and plasma etching. The key idea here is the use of a single crystal silicon layer as a 3D mask in order to utilize the different selectivity between silicon/photoresist and diamond/silicon in appropriate plasma etching conditions. A silicon-on-insulator (SOI) substrate with device layer of 3 μm was cleaned in piranha and used for silicon microlens fabrication. Figure 2 illustrates the process flow of our method. Photoresist SPR220 7.0 was spun on the Hexamethyldisilazane (HMDS)-primed SOI substrate with a speed of 4000 revolution per minute (RPM). Photolithography was used to define the photoresist microdisk patterns. A reflow technique was used to form the dome-shape
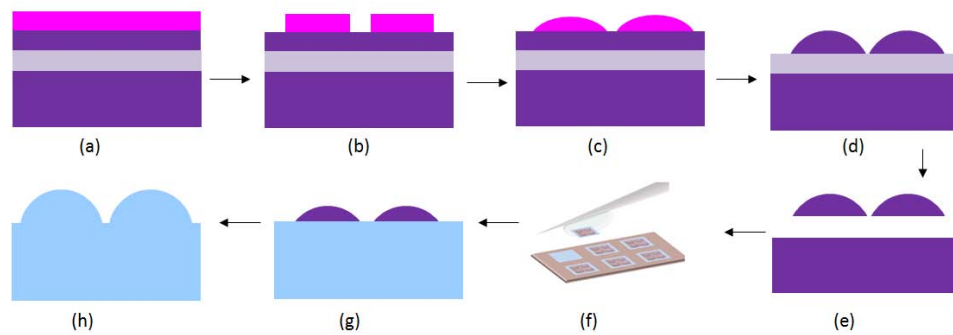
Fig. 2. Fabrication process of diamond near-hemisphere microlens: (a) photoresist was spun on an SOI substrate; (b) photoresist microdisk was patterned; (c) reflowed photoresist microlens; (d) plasma etched silicon microlens; (e) BOE etched SOI substrate, buried oxide layer removed; (f-g) PDMS tip-based pick-and-place transfer technique was used to move the suspended silicon microlens array onto a diamond substrate; (h) diamond near hemisphere microlens are etched down using silicon thin film mask.

photoresist microlens from the microdisk. Plasma etching was used to transfer the photoresist microlens into silicon device layer. The buried oxide was removed by buffered oxide etch (BOE), leading to a suspended silicon mask shown in Fig. 3(c). We than used Polydimethylsiloxane (PDMS) tip to transfer the suspended silicon microlens array onto a Sumicrystal single crystalline diamond substrate with diameter and thickness of 3 mm and 1 mm, respectively. A second plasma etching process was used to transfer the silicon microlens structures into diamond and thus diamond near hemisphere microlens were fabricated.

Figure 3(a) shows the optical images of photoresist microlens. The photoresist microlens was produced by reflow technique. Firstly, the photoresist pillar was patterned by photolithography. Then, it was baked at 140 °C for 20 min and the photoresist pillar was changed to dome shape due to surface tension and gravity. Finally, the substrate was hard baked at 190 °C for 1 hour. Figure 3(b) shows the measured curve of photoresist microlens surface profile, of which height is about 7 μm and its diameter is 38 μm. The dome pattern was transferred to device layer of the SOI substrate via plasma etching (RF power 100 W). Using O_2 and SF_6 as etching gases, flow rates of O_2 and SF_6 were 20 and 25 sccm, respectively. Figures 3(c) and 3(d) show the fabricated silicon microlens and its measured surface profile, respectively. The height of silicon lens is about 2.2 μm, which can be tuned by changing ratio between O_2 and SF_6.

A pick-and-place method [44] using PDMS adhesive was applied to transfer the silicon microlens onto diamond substrate as a contact etch mask. As shown in Fig.4(a), we have successfully placed masks firmly to the diamond substrate surface. The silicon mask was 100 μm × 100 μm in area. The silicon microlens pattern was transferred to diamond substrate using an inductively coupled plasma (ICP) reactive-ion etching (RIE) etching with $O_2/SF_6/Ar$ recipes. The flow rates of O_2 and Ar were 40 sccm and 15 sccm (a chamber pressure of 7 mTorr), respectively. Figure 4(b) shows an SEM image of the fabricated single crystal diamond microlens with smooth surface.

Note that the etching pits occur in the open area around the lens. They usually have a round shape. These round etching pits are different from the pyramidal or triangular etch pits [45]. It is relatively common in diamond deep plasma etching [46]. One possibility is that such etching pits are produced through micro-masking and trenching in the plasma etching process. Small portion of the hard mask is etched away and redeposited on the open area. Subsequently, those redeposited micro-masks are severed as etching masks and form round-shape trenching. The trenching generally occurs close to the bottom of diamond microlens/waveguides when etching
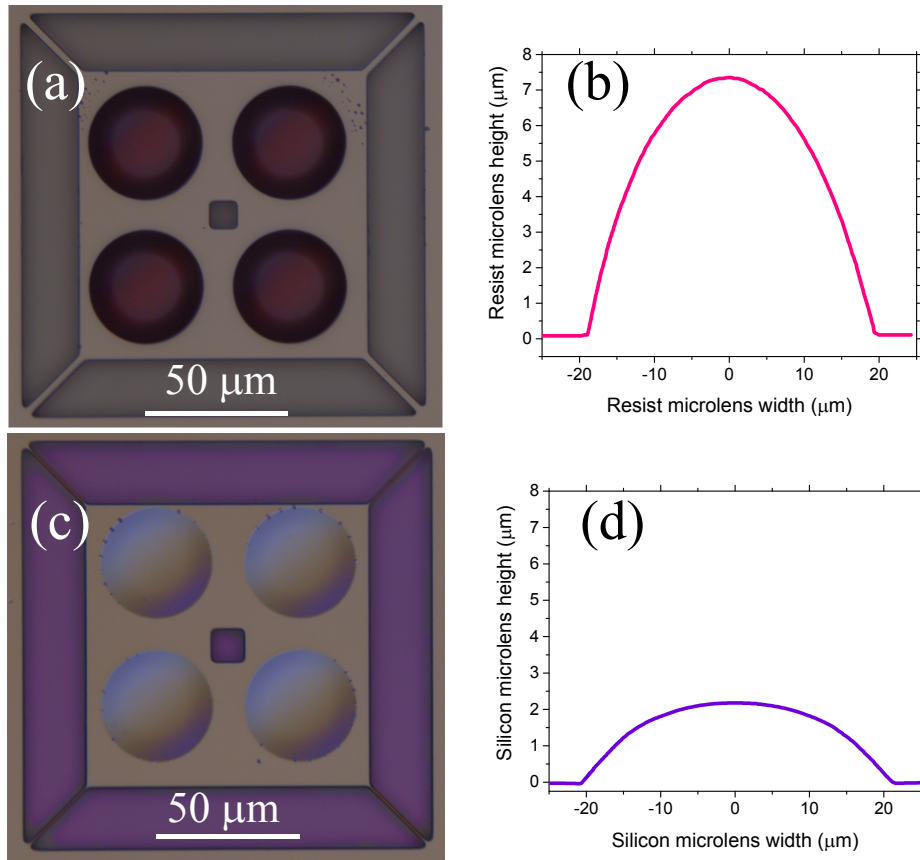
Fig. 3. Photoresist microlens and silicon microlens: (a) optical image of photoresist microlens; (b) measured surface profile of photoresist microlens; (c) optical image of silicon microlens; (d) measured surface profile of silicon microlens.
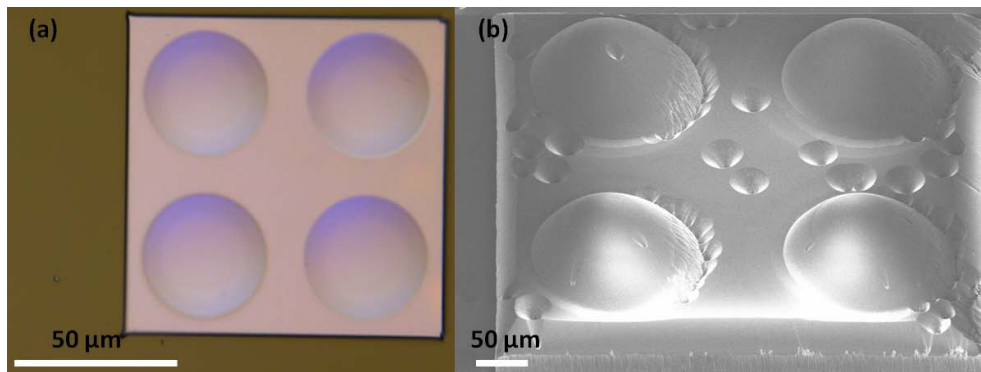

Fig. 4. Fabricating diamond microlens: (a) silicon mask on diamond substrate; (b) fabricated diamond microlens.
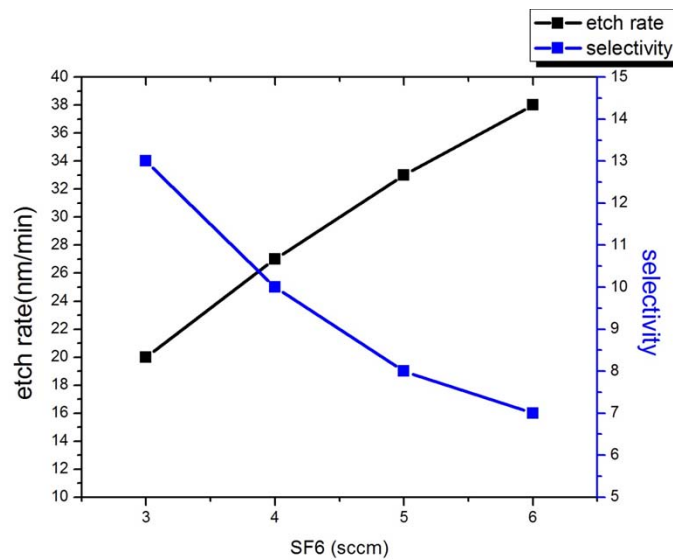
Fig. 5. Etching rate of silicon and selectivity between diamond/silicon under different gas mixtrues.

with a strong bias [47]. In the open area, the surface experiences a much longer etching time, thus resulting in a higher percentage of etching pits.

Selectivity between diamond and silicon can be as high as 40 as reported in literature [44]. Increasing flow rate of sulfur hexafluoride (SF_6) can reduce the diamond/silicon selectivity so that we can tune the diamond/silicon selectivity by only changing the SF_6 flow rate. As shown in Fig.5, we have studied the influence of SF_6 flow rate to silicon etching rate and diamond/silicon selectivity quantitatively. By varying the etching gas mixtures, we have found various recipes that give selectivity from 7 to 13 between diamond and silicon. In the meantime, the silicon etching rate varies from 20 nm/min to 38 nm/min.

As shown in Fig.6, by changing the SF_6 flow rate we have fabricated diamond microlens with height varying from 10 μm to 19 μm. Ellipsoid curve has been used to fit the surface profile measurement data sets and the h/r varies from 0.69 to 1.15. The overall fitting is satisfactory. The disparity on the feet of the diamond microlens is relatively large which is mainly due to the measurement error of the surface profiler tip. Since all the h/r values are larger than 0.64, it thus can be concluded that the maximum value of θ is smaller than the total reflection critical angle.

As diamond microlens height increases, its diameter increases from 36 μm to 40 μm, while keeping the smoothness of its surface. Atomic force microscope (AFM) measurement is taken at the top of the diamond microlens using PeakForce Tapping mode of Bruker Dimension FastScan model. The AFM image (raw data) is shown in Fig. 7(a) and the flattened result is shown in Fig. 7(b). The values of mean roughness and root mean square roughness can be estimated to 2.1 nm and 1.6 nm at the top of the measured diamond microlens with area of 2 μm $\times$ 2 μm, respectively.

4. Conclusion

In summary, we have successfully fabricated single crystal diamond microlenses with smooth surface via a 3D mask transfer method. We have systematically study the relationship between gas mixture ratio and diamond/silicon selectivity. We have derived the condition that is required to meet in order to avoid total internal reflection, in which the height of diamond microlens should
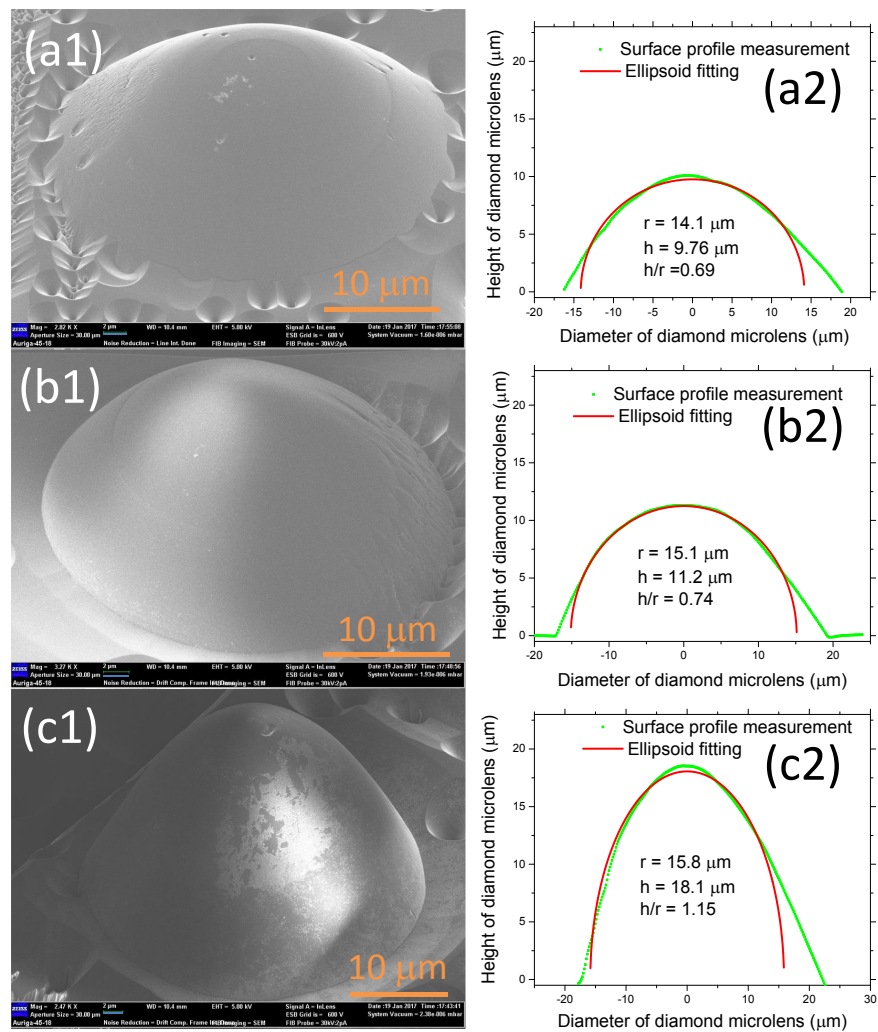
Fig. 6. Diamond microlens with various heights [(1) SEM images and (2) surface profile measurements with ellipsoid fitting results]: (a) height: 10 μm, SF$_6$ flow rate: 6 sccm; (b) height: 12 μm, SF$_6$ flow rate: 5 sccm; (c) height: 19 μm, SF$_6$ flow rate: 3 sccm.
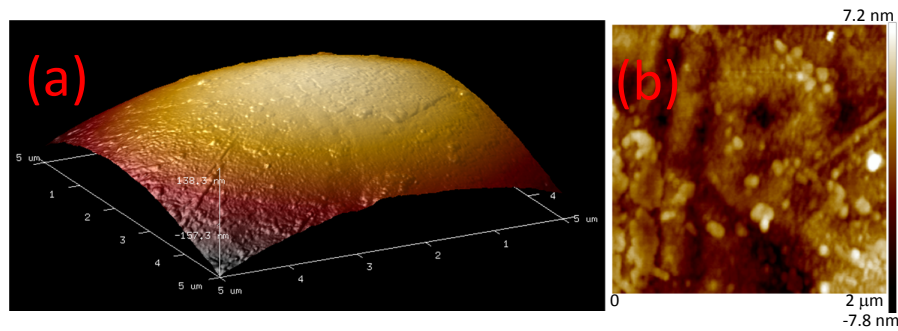
Fig. 7. AFM measurement on top of a diamond microlens: (a) the scanned result showing a curved microlens surface; (b) flattened result where the microlens curve surface (reference background) has been subtracted.

be larger than 0.64 times its radius. Our method utilizes standard cleanroom microfabrication processes including photolithography, photoresist reflow, and plasma etching. Thus this scalable approach could also be used to fabricate other diamond microstructures, such as spiral phase plate and negative X-ray refractive lens.